Voltage-gated proton channel in a dinoflagellate

Susan M. E. Smith[a], Deri Morgan[b], Boris Musset[b], Vladimir V. Cherny[b], Allen R. Place[c], J. Woodland Hastings[d,1], and Thomas E. DeCoursey[b,1]

[a]Department of Pathology, Emory School of Medicine, Atlanta, GA 30322; [b]Department of Molecular Biophysics and Physiology, Rush University Medical Center, Chicago, IL 60612; [c]Institute of Marine and Environmental Technology, University of Maryland Center for Environmental Sciences, Baltimore, MD 21202; and [d]Department of Molecular and Cellular Biology, Harvard University, Cambridge, MA 02138

Contributed by J. Woodland Hastings, September 21, 2011 (sent for review August 25, 2011)

Fogel and Hastings first hypothesized the existence of voltage-gated proton channels in 1972 in bioluminescent dinoflagellates, where they were thought to trigger the flash by activating luciferase. Proton channel genes were subsequently identified in human, mouse, and *Ciona intestinalis*, but their existence in dinoflagellates remained unconfirmed. We identified a candidate proton channel gene from a *Karlodinium veneficum* cDNA library based on homology with known proton channel genes. *K. veneficum* is a predatory, nonbioluminescent dinoflagellate that produces toxins responsible for fish kills worldwide. Patch clamp studies on the heterologously expressed gene confirm that it codes for a genuine voltage-gated proton channel, kH_V1: it is proton-specific and activated by depolarization, its g_H–V relationship shifts with changes in external or internal pH, and mutation of the selectivity filter (which we identify as Asp^{51}) results in loss of proton-specific conduction. Indirect evidence suggests that kH_V1 is monomeric, unlike other proton channels. Furthermore, kH_V1 differs from all known proton channels in activating well negative to the Nernst potential for protons, E_H. This unique voltage dependence makes the dinoflagellate proton channel ideally suited to mediate the proton influx postulated to trigger bioluminescence. In contrast to vertebrate proton channels, whose main function is acid extrusion, we propose that proton channels in dinoflagellates have fundamentally different functions of signaling and excitability.

ion selectivity | ion channel | permeation | channel gating | action potential

In many areas, when ocean water is disturbed at night, it sparkles with distinctive blue light flashes discharged by bioluminescent dinoflagellates such as *Noctiluca miliaris* and *Lingulodinium polyedrum* (formerly *Gonyaulax polyedra*). Such unicellular organisms contain numerous discrete light sources (1, 2), which are small organelles called scintillons (3, 4). An action potential in *Noctiluca* (5, 6) was shown in the works by Eckert and Reynolds (1), Eckert (7), and Eckert and Sibaoka (8) to trigger the bioluminescent flash. On mechanical stimulation (e.g., a breaking wave or wake of a ship), an action potential travels across the membrane of the large central flotation vacuole, the tonoplast (7), and invades the scintillon membrane, which is continuous with the tonoplast. The vacuolar sap is at pH 3.5 (9), resulting in a large chemical driving force for protons to enter the scintillons through hypothetical proton channels (10). Proton entry into the scintillon triggers the flash by two concerted mechanisms: low pH activates luciferase itself (11, 12) and also causes release of the substrate luciferin from luciferin binding protein (11, 13–15). The action potential peak decreases when the vacuolar pH is increased (16), suggesting that, in addition to triggering the flash, proton channels may mediate the action potential (17).

Here, we report the discovery of a gene for a voltage-gated proton channel in a dinoflagellate, *Karlodinium veneficum* (synonymous with *Gymnodinium veneficum*) (18), one of the few dinoflagellate species for which a sequence library is available. *K. veneficum* produces a variety of potent toxins (19, 20) that facilitate its predatory lifestyle by immobilizing its prey (21). These toxins are responsible for fish kills during blooms (22). In addition, this species was recently proposed as a source of biodiesel production (23).

Our goal was to identify a dinoflagellate proton channel gene, express the protein heterologously, characterize the electrophysiological properties of the protein, and compare key structural elements with those elements in known proton channels. The proton channel described here shares enough signature elements that we could identify the gene, but the protein in heterologous mammalian expression systems exhibited unique properties that suggest that voltage-gated proton channels in dinoflagellates serve radically different functions than in mammalian and other species.

Results

To identify a gene for a voltage-gated proton channel in dinoflagellates, we searched a cDNA library from *K. veneficum* (National Science Foundation Microbial Genome Sequencing Program). Although analysis of a large alignment of voltage sensor domains (VSDs) identified only a handful of sequence elements unique to the H_V1 family, H_V1s occupy a branch of a phylogenetic tree distinct from branches comprising the close homologs C15orf27 and voltage-sensitive phosphatases (VSPs) (24). To capture features of the S1–S4 transmembrane helices that comprise the core structure of the VSD, we constructed sequence logos (25) based on a multiple sequence alignment of 37 H_V1s with 15 C15orf27s, 11 VSPs, and 38 K_Vs (Fig. 1). The logos highlight differences between the various families in spacing, identity, and level of conservation of positions in each transmembrane (TM) helix and reveal some sequence patterns unique to the H_V1 family, which presumably correlate with functions not shared by other VSDs. In addition, we noticed that H_V1 C-terminal domains are significantly shorter than the domains of other VSD-containing orthologs (Fig. 1).

Using the amino acid sequences of *Ciona intestinalis* H_V1 as a probe, we used tBLASTn to search sequence libraries of full-length splice leader-primed cDNAs of *K. veneficum*; these libraries are especially deep, estimated to represent ~80% to 90% of the genes in the *K. veneficum* genome. The search identified a candidate proton channel gene, which we call kH_V1, in a cDNA library from dark-feeding *K. veneficum*. The protein sequence exhibits a good, although imperfect, match to the sequence patterns found in bona fide H_V1s (Fig. 1), giving us enough confidence to proceed. The use of cDNA rather than genomic sequence information provides very high confidence that the predicted protein sequence corresponds to the sequence expressed in the organism. Expres-

Author contributions: S.M.E.S. performed sequence analysis, identified the putative gene, and made mutants; A.R.P. searched a cDNA database and performed RT-qPCR; D.M., B.M., and V.V.C. conducted patch clamp experiments and data analysis; S.M.E.S., A.R.P., J.W.H., and T.E.D. designed research; and S.M.E.S. and T.E.D. wrote the paper.

The authors declare no conflict of interest.

Data deposition: The data reported in this paper have been deposited in the Gene Expression Omnibus (GEO) database, www.ncbi.nlm.nih.gov/geo (accession no. JN255155).

[1]To whom correspondence may be addressed. E-mail: hastings@fas.harvard.edu or tdecours@rush.edu.

This article contains supporting information online at www.pnas.org/lookup/suppl/doi:10.1073/pnas.1115405108/-/DCSupplemental.

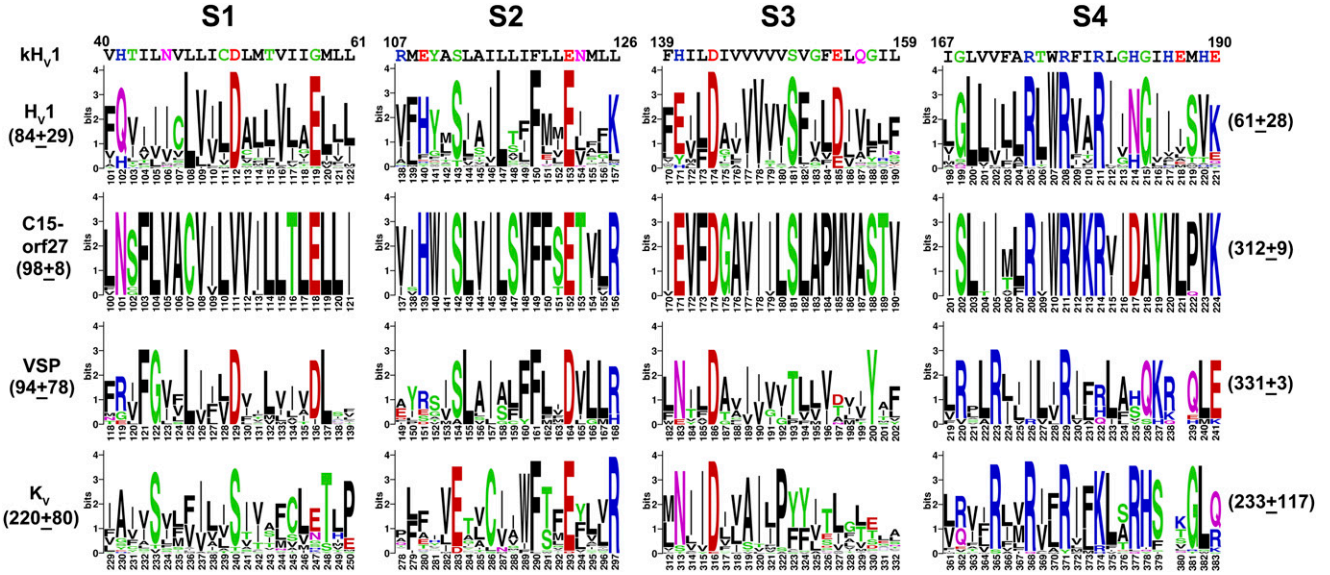

Fig. 1. The primary sequence of kH_V1 (line 1) compared with sequence logos of TM regions S1 to S4 of families of homologs that were created as described in *Materials and Methods*. The height of each letter in a stack indicates its relative representation at that location. The total stack height at each position indicates its information content, which for proteins, has a theoretical maximum of 4.3 bits (25) and depends both on the number of sequences in the alignment and the number of substitutions observed at a position. Numbers on the left and right sides indicate the length of N and C termini, respectively, (mean ± SD) of the sequences included in the alignment from which the logos were created (H_V1 $n = 37$, C15orf27 $n = 15$, VSP $n = 11$) or in the case of K_V, from a subset of 13 sequences drawn at random from the 38 sequences included in the alignment. All sequences used for the logos are listed in Table S1. One-way ANOVA followed by Tukey's test indicates that the length of the H_V1 C terminus differs significantly from the length of the C terminus of each other family ($P < 0.001$). Numbering of TM residues is for hH_V1, c15orf27, CiVSP, and *Shaker* (K_V). Although kH_V1 displays some significant differences from the most common H_V1 sequence, 30 of 87 TM residues match the predominant H_V1 pattern.

sion of kH_V1 mRNA was confirmed using RT-quantitative PCR (RT-qPCR; primers in Table S2) on mRNA extracted from cultures of *K. veneficum* grown autotrophically. For reference, expression of actin was also examined. kH_V1 mRNA was detectable in all samples but at lower levels than actin (by 78- and 71-fold in the middle of the light and dark phases, respectively), consistent with the typically low abundance of ion channel mRNA.

The kH_V1 Proton Channel Carries Large Inward Currents. We used heterologous expression in standard mammalian systems for characterization of the candidate kH_V1 and site-directed mutagenesis studies. Because dinoflagellates exhibit a significantly different pattern of codon use than mammals (26), we ordered the commercial synthesis of a gene coding for the same protein sequence but with a DNA sequence optimized for human expression cloned into a mammalian expression plasmid. Two mammalian cell lines, HEK-293 or COS-7, were transfected with kH_V1, and membrane currents were examined by tight seal voltage clamp. The family of currents recorded during a series of depolarizing voltage pulses in Fig. 2*A* reveals the most distinctive feature of kH_V1 currents. The proton conductance, g_H, activated well negative to the reversal potential, V_{rev}, and therefore, inward currents were observed over a wide voltage range. The corresponding current–voltage relationship in Fig. 2*B* is reminiscent of analogous curves for voltage-gated sodium channels. All previously described voltage-gated proton channels open only when the electrochemical gradient for protons is outward, and therefore, only outward current is observed (27).

The kH_V1 Proton Channel Is Perfectly Proton-Selective. The ion species that permeates a channel can be identified by comparing the zero current potential (V_{rev}) with the Nernst potential for each ion present. The negative range of kH_V1 activation enabled measuring V_{rev} directly in families of currents. Fig. 2*C* illustrates that V_{rev} was very close to the Nernst potential for protons, E_H, over a wide range of external pH (pH_o 4.5–8.5) and internal pH (pH_i 5.5–8.5). In fact, kH_V1 seems to be even more proton-selective than other H_V1s, although the small deviations of V_{rev} from E_H in the latter are considered to reflect imperfect pH control rather than finite selectivity for other ions (27). We suspect that the proximity of V_{rev} to E_H in kH_V1 reflects the ability to measure V_{rev} without applying a prepulse to first activate the conductance. In other species, H^+ efflux during the prepulse changes local pH sufficiently to shift V_{rev} a few millivolts positive to E_H.

Gating of the kH_V1 Proton Channel Is Regulated by the pH Gradient. A property shared by every H_V1 thus far identified is the exquisite regulation of the absolute position of the proton conductance–voltage (g_H-V) relationship by the pH gradient, ΔpH, defined as $pH_o - pH_i$. The g_H–V relationship shifts negatively by 40 mV/unit increase in pH_o or decrease in pH_i (27, 28). Fig. 3 illustrates that kH_V1 behaves in the same way. The effect of changing pH_i at constant pH_o was studied in inside-out patches of membrane (Fig. 3 *A*–*C*). The corresponding g_H–V relationships in Fig. 3*E* reveal that, at lower pH_i, channel opening occurs at more negative voltages. Activation was substantially faster at lower pH_i as in other cells (29). In addition, the limiting g_H approximately doubles per unit decrease in pH_i, consistent with H^+ rather than OH^- flux (in the opposite direction). When pH_o was varied in whole-cell measurements, the g_H–V relationship also shifted ~40 mV/unit, with little change in the maximum g_H. Thus, the effects of changes of pH_o and pH_i on the g_H–V relationship in kH_V1 are quite similar to the effects in other proton channels. In most respects, the properties of kH_V1 resemble the properties of other proton channels.

However, kH_V1 is unique in one key respect. At each pH_i studied, inward current was activated well negative to E_H (Fig. 3 *A*–*C*), which is also evident in current voltage curves (Fig. 3*D*). This negative voltage range of activation, resulting in inward current, is unprecedented. In Fig. 3*F*, the voltage at which kH_V1 current is first evident, $V_{threshold}$, is plotted against V_{rev}. In every

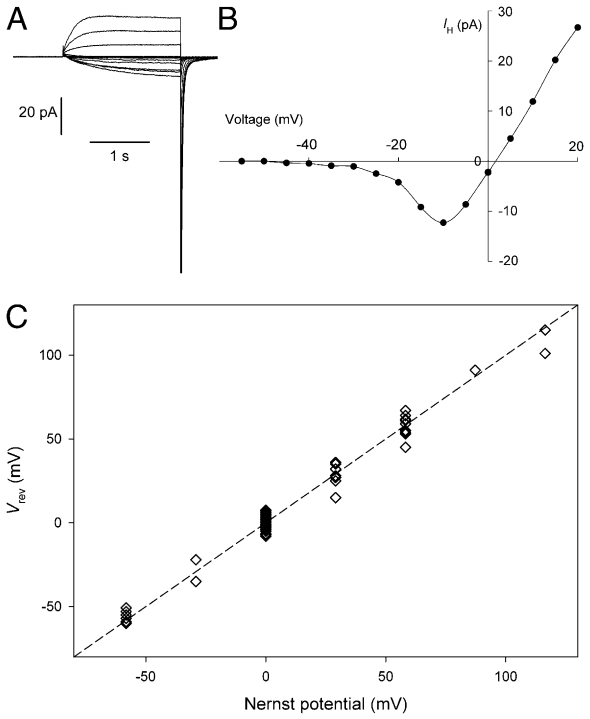

Fig. 2. The kH_V1 gene product is a voltage-gated proton channel. (*A*) Voltage-gated proton currents generated by kH_V1 in an inside-out patch from a HEK-293 cell at $pH_o = pH_i = 7.0$ during voltage pulses applied from a holding potential of −60 mV in 5-mV increments from −55 to +15 mV. (*B*) The current–voltage relationship from this family illustrates that inward currents occur over a wide voltage range negative to the Nernst potential for protons, E_H. (*C*) The measured V_{rev} is extremely close to E_H. V_{rev} was determined directly from the reversal of current during depolarizing pulses. Data from 79 whole-cell and excised patch measurements are included. The dashed line shows E_H.

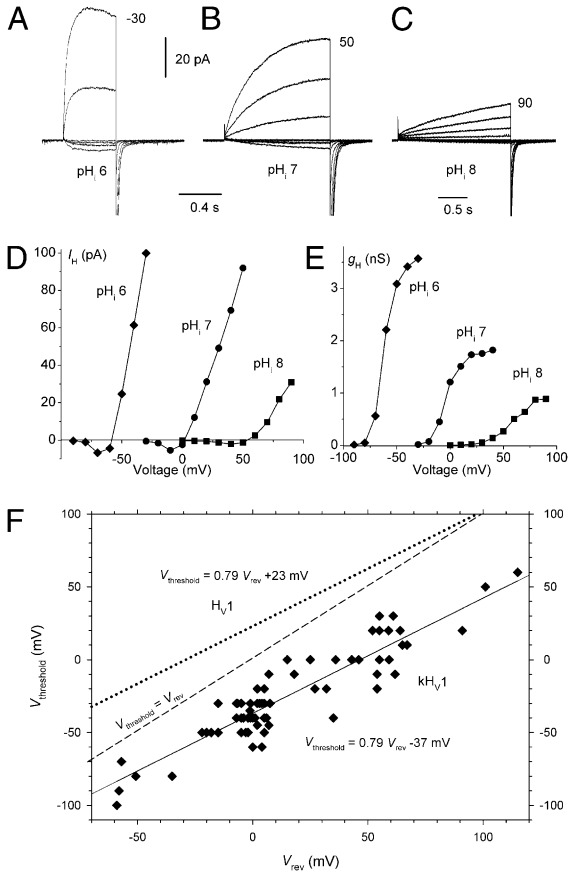

Fig. 3. Effects of pH_i on proton currents in an inside-out patch of membrane at $pH_o = 7.0$ (*A–E*) and regulation of the g_H–*V* relationship in kH_V1 by the pH gradient ΔpH (*F*). Pulses were applied in 10-mV increments up to the voltage shown at the indicated pH_i from a holding potential of −90, −60, or −40 mV for *A* to *C*, respectively. (*D*) Steady state current–voltage relationship for the families in *A–C*. The current amplitude was obtained from single exponential fits. (*E*) Corresponding g_H–*V* relationships. (*F*) The voltage at which H^+ current was first detectable (typically ~1% of the maximum g_H), $V_{threshold}$, is plotted against the V_{rev} measured in each solution in each cell or patch studied. The dashed line indicates equality between the parameters. The solid line is the least squares fit to the data given by $V_{threshold} = 0.79\ V_{rev} - 37$ mV. The dotted line shows the relationship found previously for 15 cell types (27) described by $V_{threshold} = 0.79\ V_{rev} + 23$ mV.

cell at all ΔpH explored, $V_{threshold}$ was negative to V_{rev} (the dashed line in Fig. 3*F* shows equality). Consequently, inward proton currents occur over a wide voltage range. In contrast, other proton channels are regulated by ΔpH in such a way that they conduct only outward current over the entire physiological pH range (27). The dotted line in Fig. 3*F* shows the average relationship reported for voltage-gated proton channels in 15 different types of cells (27). These relationships can be described simply by (Eq. **1**)

$$V_{threshold} = \text{slope} \times V_{rev} + V_{offset}, \qquad [1]$$

in which V_{offset} is $V_{threshold}$ at symmetrical pH. For example, when $pH_o = pH_i$, native proton currents activate 23 mV positive to V_{rev}, whereas kH_V1 activates 37 mV negative to V_{rev}. The slopes of these relationships were identical, and thus, kH_V1 activates at any given ΔpH at potentials ~60 mV more negative than all proton channels described to date. The identical slope suggests that, despite the 60-mV difference in V_{offset}, a similar mechanism is involved in the regulation of gating by ΔpH in H_V1 from all species. The profound difference in $V_{threshold}$ portends that the function of proton channels in dinoflagellates differs fundamentally from their function in other cells. Opening kH_V1 will result in inward current that will tend to depolarize the membrane regeneratively, potentially both producing an action potential and acidifying the cytoplasm. In bioluminescent species, H_V1 would conduct protons from the vacuole into the cytoplasm, propagating the action potential, and when the action potential invades the scintillon, from vacuole into the scintillon, triggering a flash.

Aspartate[51] Is the Selectivity Filter. Recently, we reported that mutation of Asp^{112} in human H_V1 converted the channel to anion selectivity, identifying Asp^{112} as the selectivity filter (24). Our alignment (Fig. 1) predicts the corresponding residue in kH_V1 to be Asp^{51}. We mutated this Asp to Glu, Ala, Ser, or His. Fig. 4 shows that the D51A mutant was anion permeable. Whole-cell currents in symmetrical pH 5.5 TMA^+ (tetramethylammonium$^+$) $CH_3SO_3^-$ (methanesulfonate$^-$) solutions were small, but they activated at roughly the same voltage as WT channels and reversed near 0 mV (Fig. 4*A*). Replacing all external $CH_3SO_3^-$ with Cl^- increased the outward current substantially (Fig. 4*B*), consistent with Cl^- influx-mediated outward current, indicating that Cl^- is more permeant than $CH_3SO_3^-$. V_{rev} shifted to near −40 mV in the Cl^- solution (Fig. 4*C*), showing that the channel is no longer proton-selective, and in fact, it has substantial permeability to Cl^-. Fig. 4*D* summarizes the Cl^- permeability of several Asp^{51} mutants. As in hH_V1, the D51S mutant was highly permeable to Cl^-, and D51H was moderately permeable. In contrast, D51E had no detectable permeability to Cl^-, and its V_{rev} was near E_H, consistent with perfect H^+ selectivity (H^+ specificity) like the WT channel.

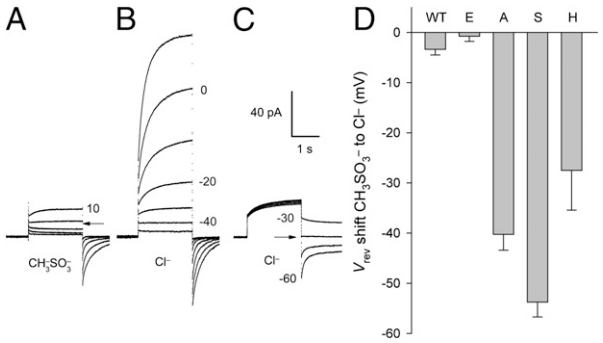

Fig. 4. Mutation of Asp^{51} alters the selectivity of kH_V1. (*A*) In symmetrical pH 5.5 TMA^+ $CH_3SO_3^-$ solutions, the whole-cell D51A conductance is activated well below 0 mV, although the inward currents are small. Pulses were applied in 10-mV increments from a holding potential of −40 mV. V_{rev} is between −10 and 0 mV (arrow). (*B*) Replacing 130 mM $CH_3SO_3^-$ with 130 mM Cl^- in the bath greatly increased outward currents during a family of pulses identical to the family in *A*. (*C*) The tail current V_{rev} in the pH 5.5 Cl^- solution was just negative to −40 mV. (*D*) Shifts of V_{rev} when $CH_3SO_3^-$ was replaced by Cl^-, all at symmetrical pH 5.5, reveal that D51A, D51S, and D51H all conduct Cl^-. Values for WT and D112E do not differ significantly from 0 mV. Error bars are SEM (n = 3, 4, 4, 4, and 4, respectively).

Structural Features of the kH_V1 Proton Channel. The relatively weak overall sequence similarity of kH_V1 to previously identified proton channels (for example, only 15% identity to hH_V1) emphasizes the generality of those features that are conserved with the rest of the H_V1 family. Several positions (L108, D112, S143, D185, L200, and W207) remain invariant in the H_V1 family (ignoring conservative D to E or S to T substitutions) but are not well-conserved across all VSD families (Fig. 1). Such positions are obvious candidates for H_V1-specific functions. Conversely, residues conserved in all other H_V1 but not kH_V1 (e.g., Glu^{119}) are evidently not essential to the H^+-specific conduction and ΔpH-dependent gating that kH_V1 exhibits. We previously showed that Asp^{185} has no direct role in the selectivity mechanism of hH_V1 (24). Positions in the VSD at which kH_V1 differs from hH_V1 (e.g., E119, K157, and E171) also seem to be unlikely candidates to participate in selectivity.

Fig. 1 highlights residues highly conserved among H_V1 family members. Some of these are also well-conserved in other VSD-containing protein families and have suggested functions in voltage sensing and gating. All four classes of VSD share conserved acidic residues in S2 and S3 TM domains (E293 and D316 in *Shaker* K_V) that are thought to act as counter charges to stabilize the S4 Arg residues when the K_V channel is open (30). This parallel construction suggests that similarly positioned acidic residues might serve a similar function in kH_V1 (E122 and D143), hH_V1 (E153 and D174), and other VSDs (Fig. 1). F290 in *Shaker* K_V was proposed to be a shielding residue in a charge transfer complex (31), and therefore, it seems reasonable that F119 in kH_V1 and F150 in hH_V1 might play a similar role.

The arginine residues in S4 spaced RxxRxxR are extremely well-conserved, and they are thought to comprise much of the voltage-sensing apparatus of VSD-containing proteins and drive S4 movement during gating of ion channels (32–37), H_V1 (38), and VSPs (39). Despite this conservation, S4 of the H_V1 family contains a different number and/or different arrangement of positive charges compared with other VSD-containing proteins, making several plausible alignments possible (40). In conjunction with an obligatory selectivity filter in S1 (Asp^{51} in kH_V1), the sequence pattern in S4, particularly, the conserved WRxxR motif, may be sufficient to identify a VSD-containing protein as H_V1. This finding suggests that, in addition to voltage sensing and movement, S4 may partake in functions specific to H_V1 and different from other VSD homologs. This interpretation is somewhat complicated by the observations that proton channels retained function after mutagenesis of individual R residues in S4 (40–42) and also after deletion of the entire C terminus starting immediately after the second Arg residue in S4 (43).

Asn^{214} was proposed to move into the narrowest portion of the conduction pathway in the open hH_V1 channel and facilitate proton conduction (44). His occupies the equivalent position in kH_V1, EhH_V1, and CpH_V1 (45). The work by Sakata et al. (43) showed that the murine equivalent N → R mutant retained proton conductance. We recently showed that N214D mutants of hH_V1 are proton-selective (24). Combined, these observations show that this position can be occupied at least by other polar residues with little obvious effect on function.

Discussion

Distinctive Properties of kH_V1. Most of the properties of kH_V1 resemble the properties of other voltage-gated proton channels. The conductance seems to be perfectly selective for protons. The channel opens with depolarization and activates more rapidly at more positive voltages. In three other species—human, mouse, and *C. intestinalis*—H_V1 seems to exist as a dimer, in which each monomer contains its own conduction pathway (44, 46–48). The dimer is held together mainly by coiled-coil interactions in the C terminus (44, 46, 48–50). The C terminus of kH_V1 lacks any predicted coiled-coil region and thus, kH_V1 may exist as a monomer. Interestingly, a putative H_V1 from *Phaeodactylum tricornutum*, a diatom, lacks a significant predicted coiled-coil region in the C terminus, whereas a weak, short region of predicted coiled coil is present in putative H_V1s from *Thalassiosira pseudonana*, another diatom, and *Trichoplax adhaerens*, a primitive single-layer multicellular organism. The C termini of two (unicellular) coccolithophore H_V1s (45) also show a region of high-probability coiled-coil interactions as do all 28 H_V1s provisionally identified by sequence similarity in multicellular species. Evidently, dimeric architecture is a feature of H_V1 in multicellular species but may be variably present in unicellular species. Dimerization slows proton channel opening (44, 48, 49); perhaps dinoflagellate H_V1s are built for speed.

The position of the g_H–V relationship depends on ΔpH in kH_V1, the same as in all other known proton channels. The slope of the V_{rev} vs. $V_{threshold}$ relationship (Fig. 3*F*) was identical, suggesting a similar governing mechanism. However, the position of the g_H–V relationship at any given ΔpH is 60 mV more negative in kH_V1 than in all other species. This unique property could reside in the sequence differences within the VSD (Fig. 1) but could also be modulated by the N or C terminus, both of which differ significantly in kH_V1 compared with other confirmed H_V1s (Fig. S1). A full explanation of this property awaits elucidation of the ΔpH gating mechanism. The functional consequence of the negatively shifted voltage dependence, however, is clear. Whereas other proton channels apparently evolved to extrude acid from cells, kH_V1 seems to be optimized to enable H^+ influx. In bioluminescent species, such as *Noctiluca*, depolarization-activated H^+ flux from vacuolar sap into the scintillon is the postulated trigger for the flash (10). A proton channel with normal properties that opens only when the proton electrochemical gradient is outward (27, 28) would not permit the H^+ influx (from the vacuole into the scintillon) required to trigger a flash. However, the uniquely negative voltage range seen in kH_V1 is perfectly suited to this task and indeed, to propagating an action potential into the scintillon membrane.

In nonbioluminescent mixotrophic species like *K. veneficum*, H^+ influx might be involved in prey digestion (e.g., signaling prey capture) or prey capture (e.g., extrusion of trichocysts). A phylogenetic analysis of VSD regions from high-confidence H_V1 sequences (Fig. S2) indicates high sequence diversity among the single-celled species and among invertebrates, suggesting the possibility of other novel functions of H_V1. As in multicellular

organisms, ion channels in dinoflagellates play various roles in regulating basic life functions, which make them targets for controlling dinoflagellate populations and behavior.

Mechanism of Proton Selectivity. Here, we identify Asp^{51} as a crucial element in the selectivity filter of kH_V1. Mutation of Asp^{51} (D51S, D51A, and D51H) converted the kH_V1 channel to anion permeability. In contrast, the conservative replacement D51E preserved proton selectivity. These results are closely analogous to the effects of Asp^{112} mutation in hH_V1 (24). In addition to identifying a residue crucial to proton selectivity in each channel, our results generalize two surprising results from the previous study in hH_V1: (*i*) a perfectly proton-selective channel can be made anion-permeable by mutation of a single amino acid, and (*ii*) replacement of Asp by His did not preserve proton selectivity. The latter point is remarkable in view of several examples of proton-conducting molecules in which His seems to be the residue responsible for proton selectivity. The M_2 viral proton channel loses its proton selectivity when His^{37} is mutated (51, 52). Even more remarkable, Arg → His mutations to the K^+ channel VSD (53, 54) or the Na^+ channel VSD (55) produce a proton-selective conductance pathway. Extensive measurements led to the conclusion that, in the Arg → His mutations to the K^+ channel VSD, the His residue is located at a constriction, where it is accessible to both external and internal solutions (53, 54, 56). Given the structural parallels of other ion channel VSDs with H_V1, we envision Asp^{51} in kH_V1 to exist at or near a similar constriction at the focus of an hourglass of water molecules. The reason that His mediates proton conduction in K^+ or Na^+ channel VSDs but anion conduction in H_V1 is obscure.

There are substantial differences in sequence and even in overall architecture (e.g., major differences in N terminus, S1–S2 loop, and C terminus) between hH_V1 and kH_V1 (Fig. S1). The fact that a single amino acid substitution converts a proton-specific channel to an anion-permeable channel in both species must, therefore, reflect an essential design feature of the proton channel. There are several possible interpretations of this phenomenon. For example, after elimination of the negative charge at Asp^{51} or Glu^{51}, the remainder of the conducting pore prefers anions, which may serve as a mechanism to exclude other cations from approaching the selectivity filter. In this view, Asp^{51} then provides both charge and proton selectivity. Elucidation of the precise mechanism of H^+ selective conduction may require calculations using a structural model.

In summary, we have identified a gene encoding a voltage-gated proton channel in the dinoflagellate, *K. veneficum*. We describe key elements that comprise the signature of a proton channel that are common to all known proton channels. The gene product shares many characteristics of voltage-gated proton channels in other species, including ΔpH-dependent gating and perfect proton selectivity. We identify Asp^{51} as the selectivity filter in kH_V1. Like its counterpart Asp^{112} in human hH_V1, its neutralization results in anion selectivity, suggesting that a common selectivity mechanism is shared by diverse H_V1s. The kH_V1 proton channel is unique in one important respect—it activates at voltages 60 mV more negative than other proton channels at any given ΔpH, resulting in a large voltage range within which inward currents occur. In contrast with other proton channels with the general function of acid extrusion (27), the function of kH_V1 is evidently proton influx, which could mediate regenerative action potentials or locally acidify the cytoplasm.

Materials and Methods

Alignments and Homology. Additions were made to a previous set of H_V1s and other VSD-containing proteins (24) by searching the updated eggNOG (57) database, which uses criteria that provide high-confidence homologs. The full set of VSDs was realigned using PromalS3D (58) as previously described (24). The resulting alignment was divided into subsets corresponding to four families of homologs: H_V1, C15orf27, VSP, and K_V; members of these subsets are listed in Table S1. Sequence logos of TM regions S1 to S4 were created from the individual family alignments using the Weblogo site (59). The length of the N terminus was taken as the number of residues before the first residue in S1, and the length of the C terminus was taken as the number of residues after the last residue in S4, which was defined in Fig. 1. The lengths of the C termini were compared by one-way ANOVA followed by Tukey's test.

Both full-length and S4 regions of *C. intestinalis* and human H_V1 were used as tBLASTx probes to search a database of full-length cDNAs cloned from *K. veneficum*. Resulting sequence hits were compared with the sequence logos and the full sequence alignment of the VSD, and kH_V1 (National Center for Biotechnology Information accession no. JN255155) was identified.

Dinoflagellate Cultures. *K. veneficum* strain CCMP2778 was grown in Corning Cell Culture Flasks (150 cm^3) in 250 mL slightly modified ESAW (enriched seawater, artificial water) medium (60) at 30 psu (practical salinity units) with the concentration of Hepes reduced to 1 mM at 24 °C. The photoperiod was shifted to 14:10 light to dark light cycle with 138 $\mu E \cdot m^{-2} \cdot s^{-1}$ photon flux on the surface of the vessel closest to the light (measured with a Li-Cor QUANTUM probe attached to a Li-Cor LI-250 light meter). The dark period started at 4:00 PM Eastern Standard Time. Cell abundance was measured on a Coulter Counter (Beckman Coulter) using the narrow size range (4–30 μm). After 19 d of growth, duplicate flasks were removed at 4-h intervals starting at 4:00 AM; a 1-mL aliquot was taken from each flask to which 50 μL glutaldehyde (50%) were added to fix cells for cell counts, and the remaining culture was poured into prechilled conical centrifuge bottles. After centrifugation at 1,500 rpm (500 × *g*) for 10 min at 25 °C, the supernatant was decanted, and 1 mL TriReagent (Molecular Research Center) was added to the pellet on ice. The pellet was triturated to an even suspension, and it was placed in a 15-mL centrifuge tube and stored at 80 °C until RNA isolation.

RNA Isolation and cDNA Preparation. Total RNA from each pooled sample was prepared using TriReagent according to the manufacturer's protocol. After precipitation, the RNA was resuspended and purified using a Qiagen RNeasy column. Total RNA was quantified by UV spectroscopy and qualified on an Agilent 2100 Bioanalyzer; 1 mg total RNA from individual cultures was reverse-transcribed in triplicate using an oligod(T) primer and the RetroScript reverse transcription kit (Ambion).

qPCR Primers and Conditions. The expression of mRNA for a select number of genes was determined by RT-qPCR using primers generated from the EST sequences obtained from library screening (Table S2). At the time of sampling, the average cell density was 10,466 ± 1,374 (n = 12) cells/mL. Preliminary experiments verified that all primer/template sets showed equivalent PCR efficiency; PCR product sizes were all about 100 to 120 nt. All real-time assays were performed on an Applied Biosystems 7500 Real-Time system using the iTaq Fast SYBR Green supermix with ROX from Bio-Rad. A sample volume of 25 μL was used for all assays, which contained a one-time final concentration of SYBR green PCR master mix, nuclease-free water, gene-specific primers (400 nM final concentration), and 1 μL reverse-transcribed sample. All samples were run in triplicate using the following protocol: 95 °C for 15 min, 94 °C for 15 s, gene-specific annealing temperature (58–62 °C) for 40 s, and 72 °C for 1 min for 40 cycles followed by a gradual increase in temperature from 60 °C to 95 °C during the dissociation (melt) stage. The dissociation stage was performed to confirm the presence of a single PCR product.

Gene Expression. A version of the kH_V1 gene optimized for human codon use but preserving the amino acid sequence was commercially synthesized (GenScript); the synthesized DNA, including a 5′ BamH1 restriction site and Kozak sequence and 3′ Not1 restriction site (complete sequence in Dataset S1), was cloned commercially (GenScript) into pcDNA3.1+ (Invitrogen). We subcloned the gene by PCR into pEGFP-C3 (Clontech) using 5′ EcoR1 and 3′ BamH1 restriction sites. Site-directed mutants were created using the Stratagene Quikchange (Agilent) procedure according to the manufacturer's instructions. Clones were sequenced commercially to confirm the mutation. HEK-293 or COS-7 cells were grown to ~80% confluency in 35-mm cultures dishes. Cells were transfected with 0.4–0.5 μg appropriate cDNA using Lipofectamine 2000 (Invitrogen) or polyethylenimine (Sigma). After 6 h at 37 °C in 5% CO_2, cells were trypsinized and replated onto glass coverslips at low density for patch clamp recording the next day. We selected green cells under fluorescence for recording.

Electrophysiology. Whole-cell or excised patch variants of the patch clamp technique were carried out as described previously (61). The main pipette solution (also used externally) contained 130 mM $TMACH_3SO_3$, 2 mM $MgCl_2$, 2 mM EGTA, and 80 mM Mes titrated to pH 5.5 with ~20 mM TMAOH. In the pH 5.5 TMACl solution, TMACl replaced $TMACH_3SO_3$. Solutions at pH 7.0 had 90 mM $TMACH_3SO_3$, 2 mM $MgCl_2$ or 3 mM $CaCl_2$, 1 mM EGTA, 100 mM BES [N,N-Bis(2-hydroxyethyl)-2-aminoethanesulfonic acid], and 36 to 40 mM TMAOH. Except where noted, experiments were done at 21 °C or room temperature (20–25 °C). No leak correction has been applied to current records. V_{rev} data were corrected for liquid junction potentials measured in each solution.

ACKNOWLEDGMENTS. We are grateful to Drs. Terry Gaasterland, John Gill, Senjie Lin, Yu-Hui Rogers, and Huang Zhang, co-primary investigators with A.R.P. for National Science Foundation Microbial Genome Sequencing Program Grant EF-0626678; "Dinoflagellate full-length cDNA sequencing," which made searching the *Karlodinium veneficum* cDNA database possible. This work was supported by National Science Foundation Award MCB-0943362 (to S.M.E.S. and T.E.D.), National Science Foundation Microbial Genome Sequencing Program Grant EF-0626678 (to A.R.P.), and National Institutes of Health Grant R01GM087507 (to T.E.D.).

1. Eckert R, Reynolds GT (1967) The subcellular origin of bioluminescence in *Noctiluca miliaris*. *J Gen Physiol* 50:1429–1458.
2. Quatrefages A (1850) Observations on *Noctiluca*. *Ann Sci Natur Zool Ser*, 3:226–235 French.
3. Fogel M, Schmitter RE, Hastings JW (1972) On the physical identity of scintillons: Bioluminescent particles in *Gonyaulax polyedra*. *J Cell Sci* 11:305–317.
4. Nicolas MT, Nicolas G, Johnson CH, Bassot JM, Hastings JW (1987) Characterization of the bioluminescent organelles in *Gonyaulax polyedra* (dinoflagellates) after fast-freeze fixation and antiluciferase immunogold staining. *J Cell Biol* 105:723–735.
5. Chang JJ (1960) Electrophysiological studies of a non-luminescent form of the dinoflagellate *Noctiluca miliaris*. *J Cell Comp Physiol* 56:33–42.
6. Hisada M (1957) Membrane resting and action potentials from a protozoan, *Noctiluca scintillans*. *J Cell Physiol* 50:57–71.
7. Eckert R (1965) II. Asynchronous flash initiation by a propagated triggering potential. *Science* 147:1142–1145.
8. Eckert R, Sibaoka T (1968) The flash-triggering action potential of the luminescent dinoflagellate *Noctiluca*. *J Gen Physiol* 52:258–282.
9. Nawata T, Sibaoka T (1976) Ionic composition and pH of the vacuolar sap in marine dinoflagellate *Noctiluca*. *Plant Cell Physiol* 17:265–272.
10. Fogel M, Hastings JW (1972) Bioluminescence: Mechanism and mode of control of scintillon activity. *Proc Natl Acad Sci USA* 69:690–693.
11. Krieger N, Hastings JW (1968) Bioluminescence: pH activity profiles of related luciferase fractions. *Science* 161:586–589.
12. Schmitter RE, Njus D, Sulzman FM, Gooch VD, Hastings JW (1976) Dinoflagellate bioluminescence: A comparative study of invitro components. *J Cell Physiol* 87: 123–134.
13. Morse D, Pappenheimer AM, Jr., Hastings JW (1989) Role of a luciferin-binding protein in the circadian bioluminescent reaction of *Gonyaulax polyedra*. *J Biol Chem* 264: 11822–11826.
14. Fogel M, Hastings JW (1971) A substrate-binding protein in the *Gonyaulax* bioluminescence reaction. *Arch Biochem Biophys* 142:310–321.
15. Bode VC, Hastings JW (1963) The purification and properties of the bioluminescent system in *Gonyaulax polyedra*. *Arch Biochem Biophys* 103:488–499.
16. Nawata T, Sibaoka T (1979) Coupling between action potential and bioluminescence in *Noctiluca*: Effects of inorganic ions and pH in vacuolar sap. *J Comp Physiol* 134: 137–149.
17. Nicolas MT, Sweeney BM, Hastings JW (1987) The ultrastructural localization of luciferase in three bioluminescent dinoflagellates, two species of *Pyrocystis*, and *Noctiluca*, using anti-luciferase and immunogold labelling. *J Cell Sci* 87:189–196.
18. Bergholtz T, Daubjerg N, Moestrup Ø, Fernández-Tejedor M (2005) On the identity of *Karlodinium veneficum* and description of *Karlodinium armiger* sp. nov. (Dinophyceae), based on light and electron microscopy, nuclear-encoded LSU rDNA, and pigment composition. *J Phycol* 42:170–193.
19. Ballantine D, Abbott BC (1957) Toxic marine flagellates; their occurrence and physiological effects on animals. *J Gen Microbiol* 16:274–281.
20. Van Wagoner RM, et al. (2010) Structure and relative potency of several karlotoxins from *Karlodinium veneficum*. *J Nat Prod* 73:1360–1365.
21. Sheng J, Malkiel E, Katz J, Adolf JE, Place AR (2010) A dinoflagellate exploits toxins to immobilize prey prior to ingestion. *Proc Natl Acad Sci USA* 107:2082–2087.
22. Deeds JR, Terlizzi DE, Adolf JE, Stoecker DK, Place AR (2002) Toxic activity from cultures of *Karlodinium micrum* (=*Gyrodinium galatheanum*)(Dinophyceae)—a dinoflagellate associated with fish mortalities in an estuarine aquaculture facility. *Harmful Algae* 1:169–189.
23. Fuentes-Grünewald C, Garcés E, Rossi S, Camp J (2009) Use of the dinoflagellate *Karlodinium veneficum* as a sustainable source of biodiesel production. *J Ind Microbiol Biotechnol* 36:1215–1224.
24. Musset B, et al. (2011) Aspartate^{112} is the selectivity filter of the human voltage gated proton channel. *Nature*, in press.
25. Schneider TD, Stephens RM (1990) Sequence logos: A new way to display consensus sequences. *Nucleic Acids Res* 18:6097–6100.
26. Hsiao YY, Lin CH, Liu JK, Wong TY, Kuo J (2010) Analysis of codon usage patterns in toxic dinoflagellate *Alexandrium tamarense* through expressed sequence tag data. *Comp Funct Genomics* 2010:138538.
27. DeCoursey TE (2003) Voltage-gated proton channels and other proton transfer pathways. *Physiol Rev* 83:475–579.
28. Cherny VV, Markin VS, DeCoursey TE (1995) The voltage-activated hydrogen ion conductance in rat alveolar epithelial cells is determined by the pH gradient. *J Gen Physiol* 105:861–896.
29. DeCoursey TE, Cherny VV (1995) Voltage-activated proton currents in membrane patches of rat alveolar epithelial cells. *J Physiol* 489:299–307.
30. Papazian DM, et al. (1995) Electrostatic interactions of S4 voltage sensor in Shaker K^+ channel. *Neuron* 14:1293–1301.
31. Tao X, Lee A, Limapichat W, Dougherty DA, MacKinnon R (2010) A gating charge transfer center in voltage sensors. *Science* 328:67–73.
32. Stühmer W, et al. (1989) Structural parts involved in activation and inactivation of the sodium channel. *Nature* 339:597–603.
33. Liman ER, Hess P, Weaver F, Koren G (1991) Voltage-sensing residues in the S4 region of a mammalian K^+ channel. *Nature* 353:752–756.
34. Papazian DM, Timpe LC, Jan YN, Jan LY (1991) Alteration of voltage-dependence of Shaker potassium channel by mutations in the S4 sequence. *Nature* 349:305–310.
35. Aggarwal SK, MacKinnon R (1996) Contribution of the S4 segment to gating charge in the Shaker K^+ channel. *Neuron* 16:1169–1177.
36. Logothetis DE, Movahedi S, Satler C, Lindpaintner K, Nadal-Ginard B (1992) Incremental reductions of positive charge within the S4 region of a voltage-gated K^+ channel result in corresponding decreases in gating charge. *Neuron* 8:531–540.
37. Seoh SA, Sigg D, Papazian DM, Bezanilla F (1996) Voltage-sensing residues in the S2 and S4 segments of the Shaker K^+ channel. *Neuron* 16:1159–1167.
38. Gonzalez C, Rebolledo S, Wang X, Perez M, Larsson HP (2011) Contribution of S4 charges to gating mechanism in Hv channels. *Biophys J* 100:173.
39. Murata Y, Iwasaki H, Sasaki M, Inaba K, Okamura Y (2005) Phosphoinositide phosphatase activity coupled to an intrinsic voltage sensor. *Nature* 435:1239–1243.
40. Ramsey IS, et al. (2010) An aqueous H^+ permeation pathway in the voltage-gated proton channel Hv1. *Nat Struct Mol Biol* 17:869–875.
41. Sasaki M, Takagi M, Okamura Y (2006) A voltage sensor-domain protein is a voltage-gated proton channel. *Science* 312:589–592.
42. Ramsey IS, Moran MM, Chong JA, Clapham DE (2006) A voltage-gated proton-selective channel lacking the pore domain. *Nature* 440:1213–1216.
43. Sakata S, et al. (2010) Functionality of the voltage-gated proton channel truncated in S4. *Proc Natl Acad Sci USA* 107:2313–2318.
44. Tombola F, Ulbrich MH, Isacoff EY (2008) The voltage-gated proton channel Hv1 has two pores, each controlled by one voltage sensor. *Neuron* 58:546–556.
45. Taylor AR, Chrachri A, Wheeler G, Goddard H, Brownlee C (2011) A voltage-gated H^+ channel underlying pH homeostasis in calcifying coccolithophores. *PLoS Biol* 9: e1001085.
46. Lee SY, Letts JA, Mackinnon R (2008) Dimeric subunit stoichiometry of the human voltage-dependent proton channel Hv1. *Proc Natl Acad Sci USA* 105:7692–7695.
47. Petheő GL, et al. (2010) Molecular and functional characterization of H_v1 proton channel in human granulocytes. *PLoS One* 5:e14081.
48. Koch HP, et al. (2008) Multimeric nature of voltage-gated proton channels. *Proc Natl Acad Sci USA* 105:9111–9116.
49. Musset B, et al. (2010) Zinc inhibition of monomeric and dimeric proton channels suggests cooperative gating. *J Physiol* 588:1435–1449.
50. Li SJ, et al. (2010) The role and structure of the carboxyl-terminal domain of the human voltage-gated proton channel Hv1. *J Biol Chem* 285:12047–12054.
51. Pinto LH, et al. (1997) A functionally defined model for the M2 proton channel of influenza A virus suggests a mechanism for its ion selectivity. *Proc Natl Acad Sci USA* 94:11301–11306.
52. Venkataraman P, Lamb RA, Pinto LH (2005) Chemical rescue of histidine selectivity filter mutants of the M2 ion channel of influenza A virus. *J Biol Chem* 280: 21463–21472.
53. Starace DM, Bezanilla F (2001) Histidine scanning mutagenesis of basic residues of the S4 segment of the *Shaker* K^+ channel. *J Gen Physiol* 117:469–490.
54. Starace DM, Bezanilla F (2004) A proton pore in a potassium channel voltage sensor reveals a focused electric field. *Nature* 427:548–553.
55. Struyk AF, Cannon SC (2007) A Na^+ channel mutation linked to hypokalemic periodic paralysis exposes a proton-selective gating pore. *J Gen Physiol* 130:11–20.
56. Starace DM, Stefani E, Bezanilla F (1997) Voltage-dependent proton transport by the voltage sensor of the *Shaker* K^+ channel. *Neuron* 19:1319–1327.
57. Muller J, et al. (2010) eggNOG v2.0: Extending the evolutionary genealogy of genes with enhanced non-supervised orthologous groups, species and functional annotations. *Nucleic Acids Res* 38:D190–D195.
58. Pei J, Kim BH, Grishin NV (2008) PROMALS3D: A tool for multiple protein sequence and structure alignments. *Nucleic Acids Res* 36:2295–2300.
59. Crooks GE, Hon G, Chandonia JM, Brenner SE (2004) WebLogo: A sequence logo generator. *Genome Res* 14:1188–1190.
60. Berges JA, Franklin DJ, Harrison PJ (2001) Evolution of an artificial seawater medium: Improvements in enriched seawater, artificial water over the last two decades. *J Phycol* 37:1138–1145.
61. Musset B, et al. (2008) Detailed comparison of expressed and native voltage-gated proton channel currents. *J Physiol* 586:2477–2486.

Table S1.

The sequence of the DNA synthesized (Genscript, Piscataway, NJ) and cloned into pcDNA3.1+ for heterologous expression in primate cells is given below. Start and stop codons are in bold, restriction sites are underlined, and the Kozak sequence is in italics. The coding sequence of the synthesized DNA was optimized for human codon usage, while preserving the protein sequence predicted by the kH_V1 cDNA (NCBI accession number JN255155).

GGATCC*GCCACC***ATG**GATAGAATCCTGCATCACGCTGTCCATACTGTGCATACATCA
AAGTCCGCAAGAGACGCTGAGGGGCACGGAACCTGGCAGAGCAAGCTGAACGAAG
CCCTGAATAGCTCCAAAGTCCACACTATCCTGAATGTGCTGCTGATTTGCGACCTGA
TGACCGTCATCATTGGGATGCTGCTGGAGCAGTACTATTCTGATAGTCAGGTGCAGG
GACTGACCGAGGCCTTCAAGGACTGCCTGGAGAAACGCACATTTTGTCCCGATCCTA
GTCACCTGGCACATTACGGGAACCACGACCTGCATGAGTGGGCCGAACGAATGGAG
TATGCATCCCTGGCCATCCTGCTGATTTTCCTGCTGGAGAACATGCTGCTGGTCCTGG
CTAATGGCTGTAGATTCTTTGCAAACCCATTCCACATCCTGGACATTGTGGTCGTGGT
CGTGAGCGTGGGATTTGAACTGCAGGGCATCCTGGGAGAGGGACATGATGCAGGAA
TTGGCCTGGTCGTGTTCGCTCGGACATGGCGGTTCATCAGGCTGGGGCACGGCATCC
ACGAAATGCACGAGGAACATGAGGCCGAAGACCACGGGGAGCATCGGGTGTCAGA
TGCCGCTGGAAGCCTGGAAGCTCCCCTGCAGAAGGGCTCCTTTGAGCAGCACGCAA
AAGGCACCTCTGGGGTGCATCATGCTCGCTCACAGGCTTCAAGTAATAGAGAGGGC
AGAGAGGGATGTTGCGTCCAG**TAA**GCGGCCGC

Supporting Information

Smith et al. 10.1073/pnas.1115405108

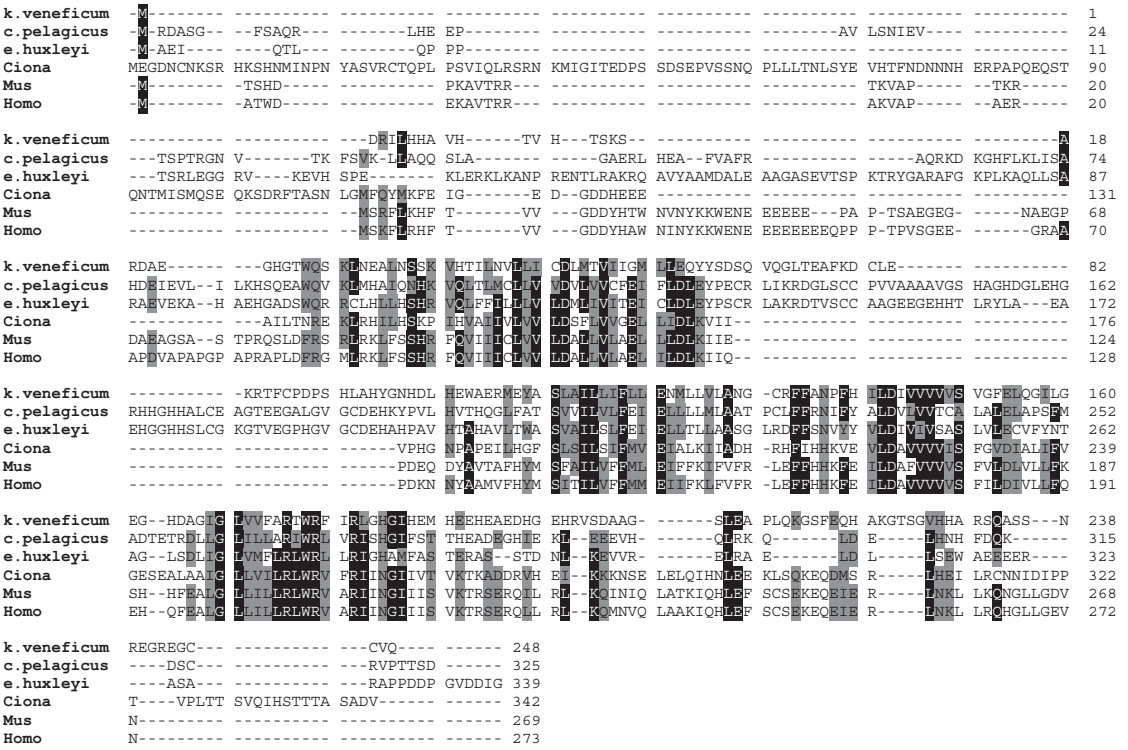

Fig. S1. Alignment of six H_V1 sequences that have been confirmed by heterologous expression and electrophysiological characterization.

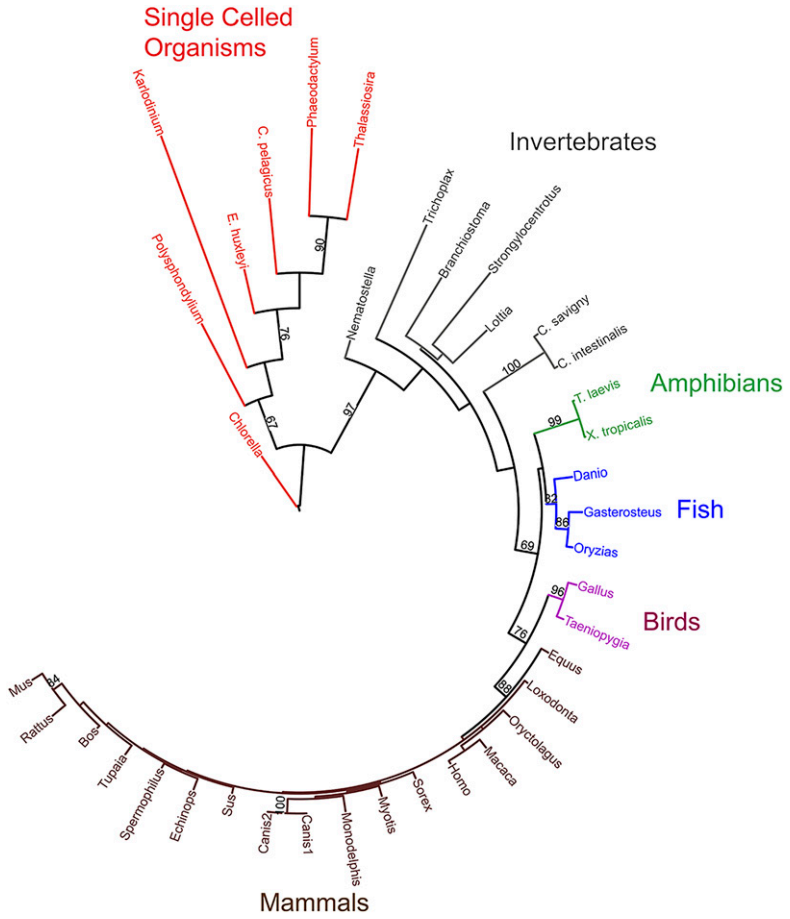

Fig. S2. Phylogenetic analysis of 37 H_V1 sequences. A maximum likelihood phylogenetic tree with 100 bootstraps was constructed using PhyML 3.0 (1) at the Mobyle portal (2) [JTT (Jones, Taylor, Thornton) substitution model, four relative substitution rate categories] from a multiple sequence alignment of the voltage sensor domain portion of 37 H_V1s. The tree was visualized using iTOL (3). Branch lengths are displayed to scale and are proportional to the distance between sequences. Bootstrap values > 60 are shown.

1. Guindon S, Gascuel O (2003) A simple, fast, and accurate algorithm to estimate large phylogenies by maximum likelihood. *Syst Biol* 52:696–704.
2. Néron B, et al. (2009) Mobyle: A new full web bioinformatics framework. *Bioinformatics* 25:3005–3011.
3. Letunic I, Bork P (2007) Interactive Tree Of Life (iTOL): An online tool for phylogenetic tree display and annotation. *Bioinformatics* 23:127–128.

Table S1. Sequences from which the family sequence logos in Fig. 1 were created

Logo	Sequences
H_V1	Homo GI:91992153; Gallus GI: 71897219; Monodelphis GI:12632423; Rattus GI: 109497399; Equus GI:194214323; Bos GI:119909285; Sus GI:194042948; Macaca GI: 109098722; Canis 1 GI:73994606; Canis 2 GI:73994604; Mus GI:109809757; Xenopus laevis GI:148235789; Xenopus tropicalis GI:58332220; Danio GI:50539752; Oryzias, ENSORLT00000025300.1; Nematostella GI: 156364735; Ciona intestinalis GI:118344228; Trichoplax GI:196002093; Branchiostoma, GI:260829267; Lottia, GI:163515737; Strongylocentrotus, GI:187282419; Ciona savigny, ENSCSAVP00000013390; Gasterosteus, ENSGACP00000001300; Loxodonta, ENSLAFP00000014329; Taeniopygia, GI:224071257; Myotis, ENSMLUP00000014199; Oryctolagus, GI:291406960; Spermophilus, ENSSTOP00000008457; Echinops, ENSETEP00000005693; Sorex, ENSSARP00000000511; Tupaia, ENSTBEP00000011847; Chlorella, GI: 307105313; Polysphondilium, GI: 281201471; E. huxleyi, jgi: 631975; C. pelagicus, GI: 304359300; Phaeodactylum GI:219120098; Thalassiosira, GI:224008803; Karlodinium (kHv1), GI: JN255155
C15orf	Ornithorhyncus GI:149410687; Danio GI:123703002; Monodelphis GI:12627230 ; Sus GI:194039682; Homo GI:118442841; Pan GI:114658268; Equus GI:149692210; Mus GI: 27370422 ; Rattus GI:157817759 ; Meleagris, GI:326926430; Taeniopygia, GI:224061716; Pongo, GI:297697189; Callithrix, GI:296236847; Ailuropodia, GI:301780212; Oryctolagus, GI: 291410741
VSP	Ciona GI:76253898; Mus GI:0549440; Homo GI:213972591; Homo GI: 40549435; Canis GI:73993164; Rattus GI:157820295; Xenopus tropicalis GI: 62859843; Xenopus laevis GI:148230800; Danio GI:70887553; Gallus GI: 118084924; Ornithorhyncus GI:149635858
K_V	Homo, sp_Q8TDN2; Homo, sp_Q9H3M0; Homo, sp_Q14721; Canis, sp_Q95167; Drosophila, sp_P17970; Pongo, sp_Q5RC10; Homo, sp_Q9BQ31; Saimiri, sp_A4K2X4; Gallus, sp_O73606; Homo, sp_Q8TDN1; Rattus, sp_Q01956; Homo, sp_Q96PR1; Drosophila, sp_P17972; Homo, sp_Q09470; Rattus, sp_P17659; Homo, sp_P22460; Rattus, sp_P15384; Canis GI: 57088651; Bos sp_Q05037; Homo sp_Q16322; Rattus GI: 16087779; Homo GI: 4826782; Rattus PDB:2A79; Canis, sp_Q28293; Drosophila, GI: 288442; Oryctolagus, sp_Q9TTT5; Aeropyrum, PDB:1ORS; Oncorhynchus, SP_Q9I830; Danio, TR_B0V2U3; Danio, TR_E0R7P8; Brugia, TR_A8NE89; Brugia, TR_A8QFU4; X. laevis, TR_Q91593; X. laevis, TR_Q91592; X. laevis, TR_B7ZRQ9; Dicentrarchus, TR_E6ZH08; Squalus, TR_O73925; Zonochria, TR_D8KW77

GI, accession numbers from the National Center for Biotechnology Information; ENS, accession numbers from Ensembl; JGI, numbers from Joint Genome Institute; TR or sp, accession numbers from Uniprot. VSP, voltage-sensitive phosphatase.

Table S2. Primers used for quantitative PCR

Primers	Sequence
Actin primers	
Kven_actin-QFor	GTTGTGCTATGTCGCTTT
Kven_actin_QRev	GCTCGTACGTTTTCTCTT
kH_V1 primers	
Kven_proton_QF1	TGGTAACCATGACTTGCACG
Kven_proton_QR1	TCACTGCACGCAACAACCTT

Other Supporting Information Files

Dataset S1 (PDF)